Histone H3.3 G34 mutations promote aberrant PRC2 activity and drive tumor progression

Jain S.U. et al., **Proc. Natl. Acad. Sci.** 2020

Supplementary Information

www.pnas.org/cgi/doi/10.1073/pnas.2006076117

Supplementary Figure 1

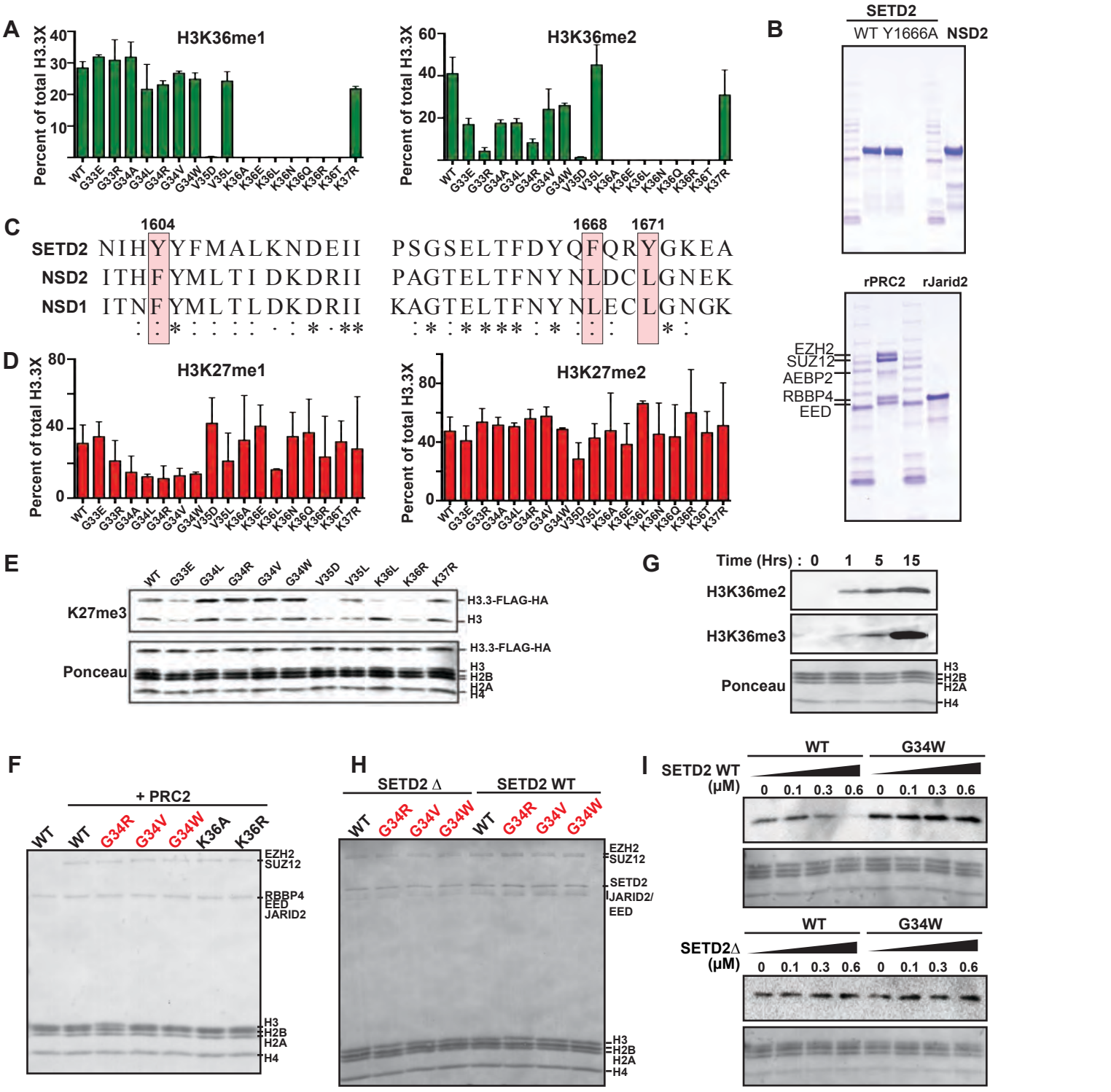

Supplement Figure 1: **(A)** Mass spectrometry data displaying the abundance of H3K36me1 and H3K36me2 on mutated peptides relative to wildtype H3.3. **(B)** Coommassie stained SDS-PAGE gel displaying the enzymes used for in vitro histone methyltransferase activity assays. **(C)** Multiple sequence alignment showing the conservation of amino acids present at the substrate tunnel of SETD2. Residues highlighted are likely sterically hindered by G34 mutations. **(D)** Mass spectrometry data displaying the abundance of H3K27me1 and H3K27me2 on mutated peptides relative to wildtype H3.3. Dashed line represents no change. **(E)** Immunoblot displaying the levels of H3K27me3 on mono-nucleosomes conataing ectopically expressed FLAG-HA-epitope tagged histones. **(F)** Ponceau staining of nucleosome substrates and PRC2 used in in vitro methyltransferase assays in Figure 1G. **(G)** Immunoblots of time course of SETD2 *in vitro* methyltransferase reactions using mono-nucleosome substrates. **(H)** Ponceau staining of nucleosome substrates and enzymes used in sequential in vitro methyltransferase assays in Figure 1I. **(I)** 300 nM nucleosome substrates were preincubated with increasing concentration of SETD2 WT or catalytic mutant SETD2 for 5 hours, followed by PRC2 for 3 hours. Immunoblots displaying the H3K27me3 on final reaction products.

Supplementary Figure 2

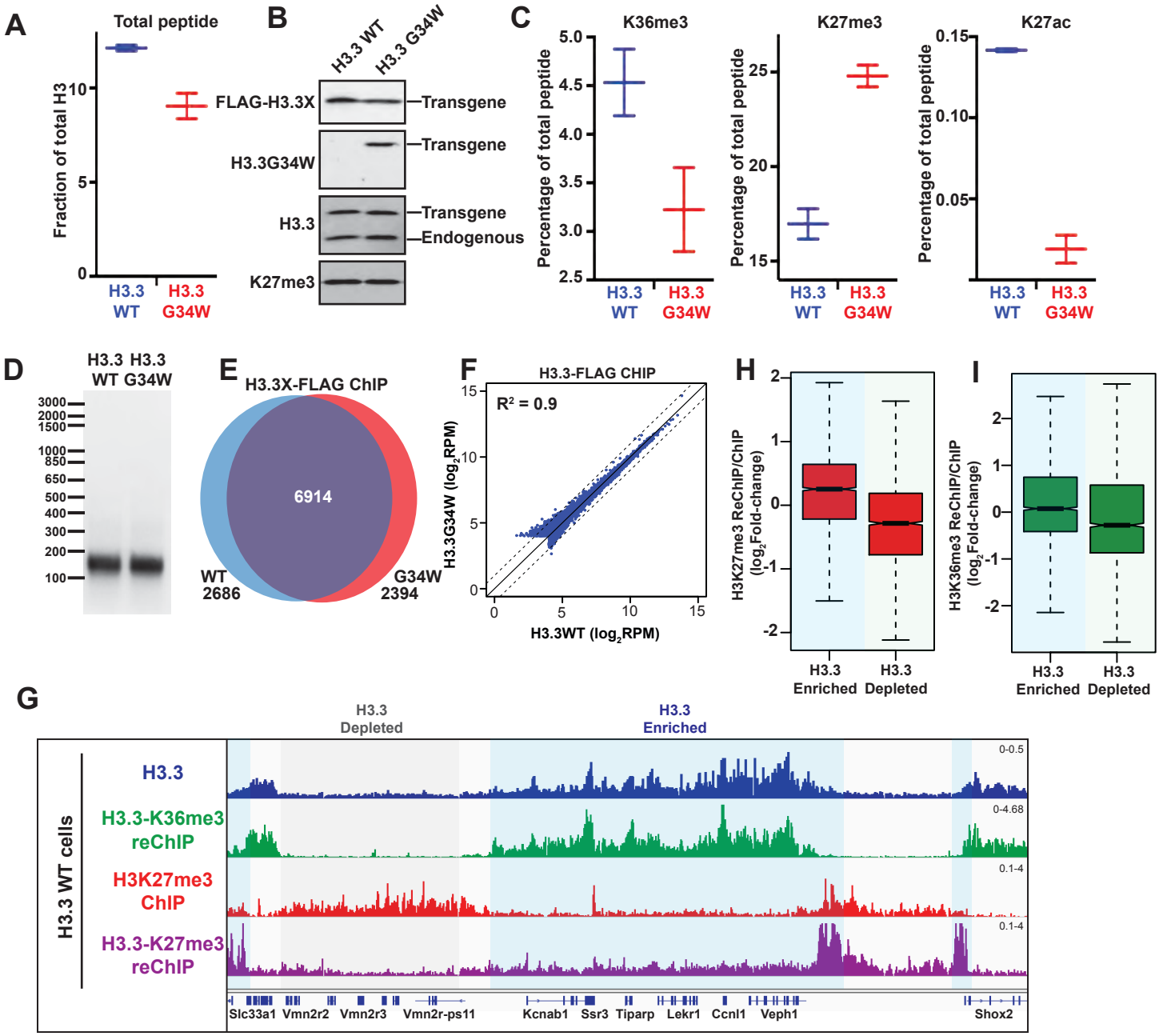

Supplementary Figure 2: (A) Mass spectrometry analysis of acid extracted histones from mMSCs expressing H3.3 G34W. Abundance of H3.3 WT or H3.3 G34W mutated peptides relative to total H3 peptide in cells expressing H3.3 G34W is displayed. **(B)** Immunoblots from whole cell lysates of C3H10T1/2 mMSCs expressing FLAG-HA epitope tagged H3.3 wildtype or H3.3 G34W. **(C)** Mass spectrometry analysis of acid extracted histones from mMSCs expressing H3.3 G34W. Abundance of H3K36me3, H3K27me3 and H3K27ac on H3.3 WT or H3.3 G34W mutated peptides is displayed as a fraction of total peptide. **(D)** A representative image of EtBr stained agarose gel displaying the fragment size distribution of DNA in input chromatin used in ChIP and reChIP experiments. DNA was purified from reverse crosslinked chromatin prior its size-resolution on a 2% agarose gel. **(E)** Venn diagram displaying the overlap between H3.3-FLAG peaks in cells expressing H3.3WT or G34W. **(F)** Scatterplot displaying the correlation between enrichment of H3.3WT and H3.3G34W histones in mMSCs at H3.3 peaks. RPM: Reads Per Million reads. R^2 value was determined from a x=y curve. **(G)** Genome browser view displaying the enrichment profile of H3.3, H3.3K36me3 reChIP, H3K27me3 ChIP and H3.3K27me3 reChIP. Blue and red boxes represent genomic loci enriched and depleted with H3.3. **(H and I)** Boxplots displaying the change in the RPKM intensities of H3K27me3 reChIP/ChIP (H) and H3K36me3 reChIP/ChIP (I) in H3.3 enriched (blue) and depleted (green) regions. Center line in the boxplots represents the median, bottom and top of the box represents 25th and 75th quartiles; whiskers extend to 1.5x interquartile range.

Supplementary Figure 3

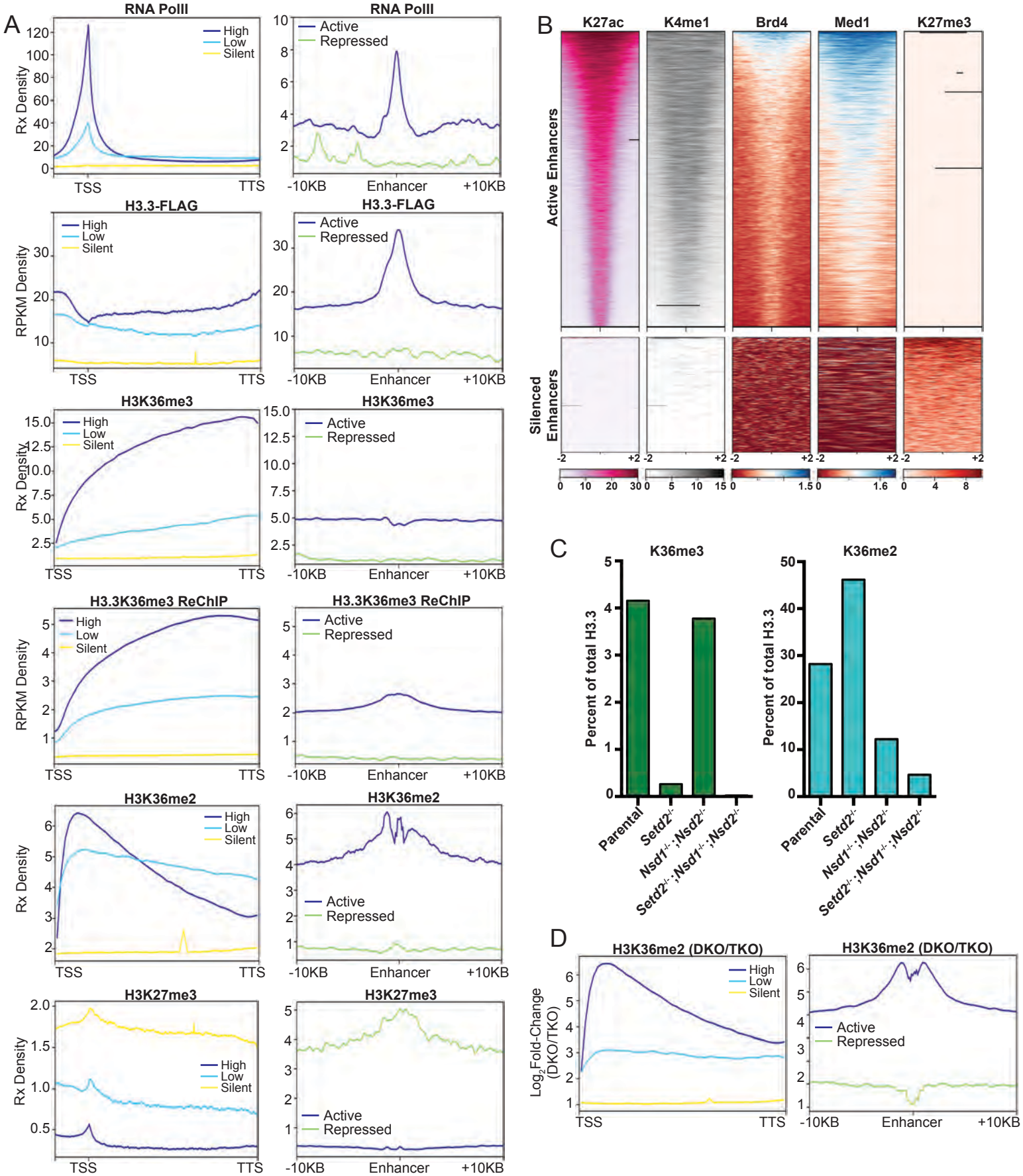

Supplementary Figure 3: (A) Average profiles of RNA Polymerase-II, H3.3-FLAG, H3K36me3 ChIP, H3.3-K36me3 reChIP, H3K36me2, H3K27me3 ChIPs at coding genes (left) and active enhancers (right) in mMSCs. Genes were classified based on their expression. High expression genes (Expression >= 400 TPM); Low expression genes (10 <= TPM < 400); Silenced genes (TPM < 10). **(B)** Active enhancers were defined by non-promoter associated H3K27ac peaks and silenced enhancers were defined by loci that had H3K27ac in embryonic stem cells but contained H3K27me3 in mMSCs. **(C)** Mass spectrometry data displaying the levels of H3K36me3 and H3K36me2 as a fraction of total H3.3 in parental, *Setd2*$^{-/-}$, *Nsd1*$^{-/-}$/ *Nsd2*$^{-/-}$, and *Setd2*$^{-/-}$/*Nsd1*$^{-/-}$/*Nsd2*$^{-/-}$ C3H10T1/2 cells. **(D)** Metagene analyses displaying SETD2-mediated H3K36me2 at coding genes (left) and active enhancers (right). SETD2-mediated H3K36me2 was identified by comparing H3K36me2 quan-

Supplementary Figure 4

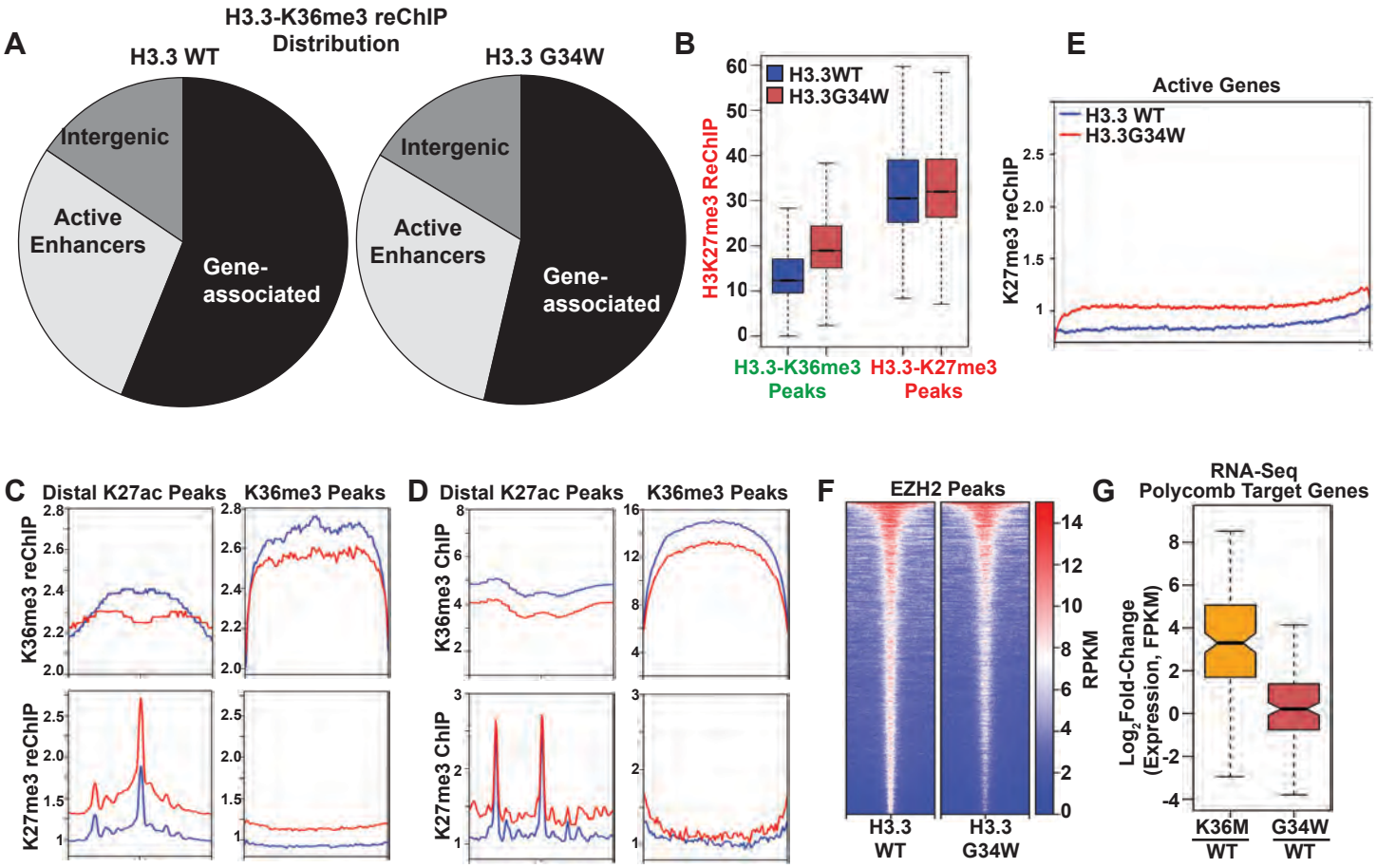

Supplementary Figure 4: **(A)** Pie chart displaying the relative distribution of H3.3-K36me3 reChIP reads within genes, enhancers or intergenic regions in cells expressing H3.3 WT or G34W. **(B)** Boxplot displaying the H3.3X-K27me3 reChIP normalized read density at H3.3-K36me3 and H3.3-K27me3 peaks respectively. **(C)** Metagene analysis displaying the average profile of H3.3-K36me3 and H3.3-K27me3 reChIP enrichments at active enhancers (distal H3K27ac peaks) and H3K36me3 peaks in cells expressing H3.3 WT (blue) or G34W (red). **(D)** Metagene analysis displaying the average profile of H3K36me3 and H3K27me3 ChIP enrichments at active enhancers (distal H3K27ac peaks) and H3K36me3 peaks in cells expressing H3.3 WT (blue) or G34W (red). **(E)** Metagene analysis displaying the average profile of H3K27me3 reChIP at active genes in cells expressing H3.3 WT or G34W (Compare with Figure 2E). **(F)** Heatmap displaying the EZH2 enrichment at EZH2 peaks. **(G)** Boxplot displaying the fold-change in the expression of polycomb-target genes in C3H10T1/2 cells expressing H3.3 K36M (orange) or H3.3 G34W (red) compared to H3.3 WT.

Supplementary Figure 5

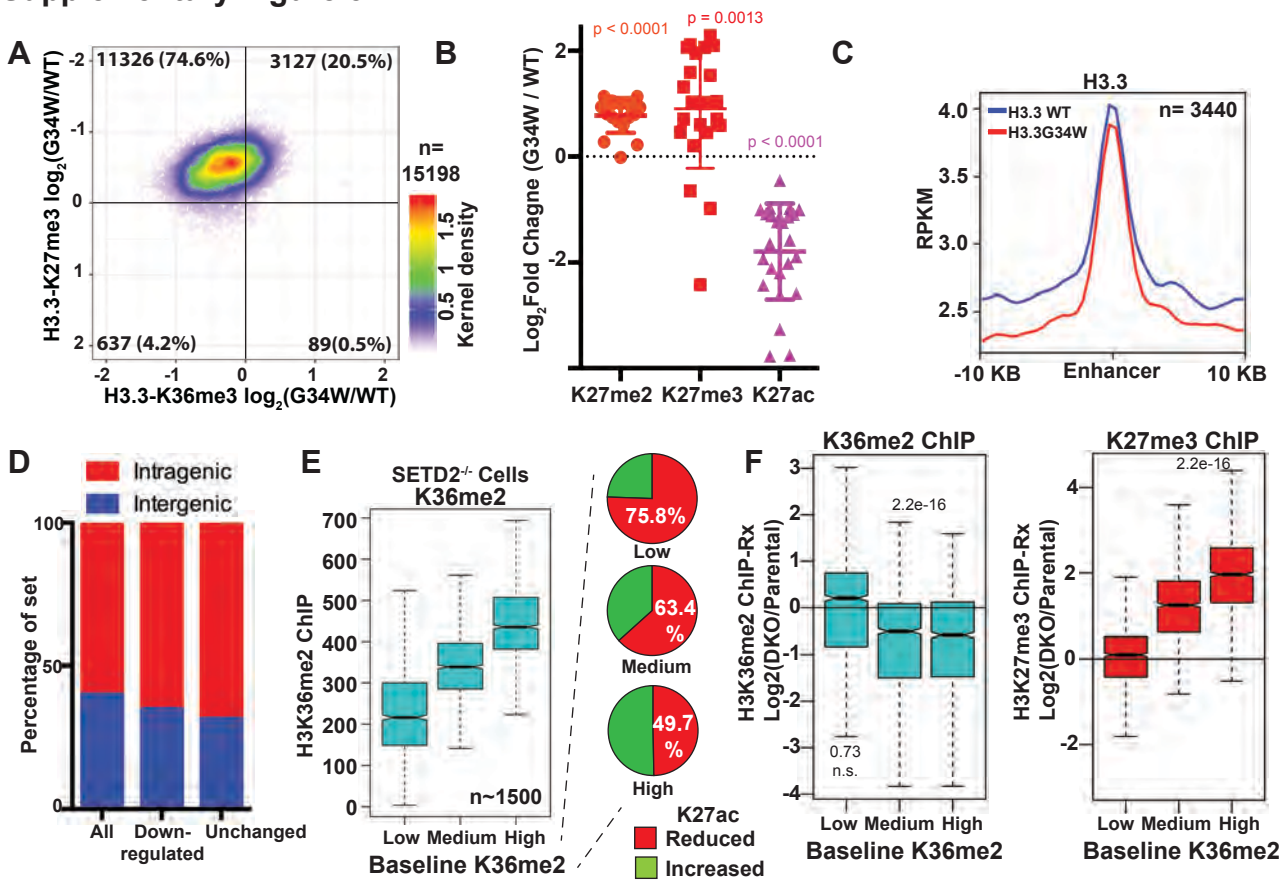

Supplementary Figure 5: (A) Scatter-plot displaying the correlation between changes in normalized H3.3-K27me3 reChIP and H3.3-K36me3 reChIP enrichments at all active enhancers shown in Figure 3A. Color key (red, yellow, green and blue) represents increasing densities of data points. **(B)** ChIP-qPCR data displaying the fold change in the enrichment (percent input) of H3K27me2, H3K27me3 and H3K27ac ChIPs at lowered enhancers. p-value was determined using t-test. **(C)** Average profiles of H3.3X-FLAG in cells expressing H3.3WT or G34W at enhancers displaying lowered H3K27ac. **(D)** Genomic distribution of all active enhancers, lowered and unchanged enhancers within inter- and intra-genic regions. **(E)** Boxplots displaying the reference-normalized H3K36me2 ChIP-Seq intensities in SETD-/- cells (NSD1/2-catalyzed H3K36me2) at enhancers containing low, medium and high levels of H3K36me2 as classified in Figure 3F. Piecharts display the fractions of enhancers within each category that had reduced H3K27ac (red). **(F)** Boxplots displaying the fold-change in H3K36me2 and H3K27me3 ChIP enrichment at enhancers containing low, medium or high levels of H3K36me2 upon NSD1/2 knockout (DKO). Depletion of NSD1/2 led to substantial loss of H3K36me2 and gain of H3K27me3 at "NSD1/2-protected: enhancers containing high H3K36me2. p-values were determined using Wilcoxon's rank sum test.

Supplementary Figure 6

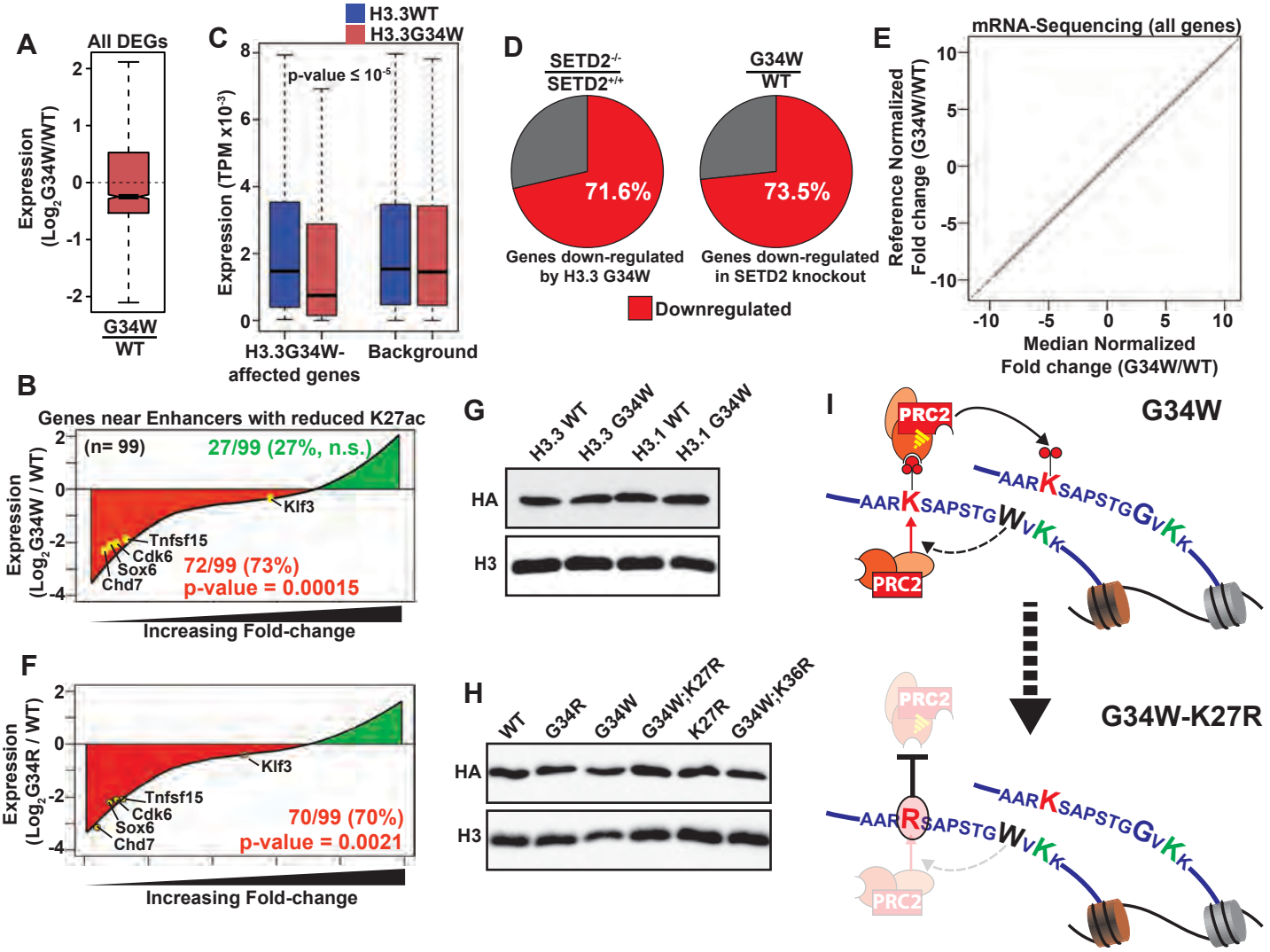

Supplementary Figure 6: (A) Boxplot displaying the fold-change in the expression of all differentially expressed genes (PPDE ≥ 0.95, No fold-change cutoff, n= 2121). **(B)** Fold change in the expression of genes associated with at least three lowered enhancers as defined in Figure 4A is plotted against their percentile. Genes implicated in cell fate determination are highlighted in yellow. p-values of enrichment of up- and down- regulated genes were determined using randomization test. **(C)** Boxplot displaying the expression of H3.3 G34W-affected genes near enhancers with reduced H3K27c (as defined in 4A) compared to all genes with PPDE ≥ 0.95. p-value of downregulation of G34W-affected genes was determined using randomization test. **(D)** Pie charts displaying the effect of SETD2 knockout on H3.3 G34W-downregulated genes (left) or vice versa (right). **(E)** Scatterplot displaying the fold-change (G34W/WT) in the expression of all genes normalized by exogenous reference (y-axis) and internally median normalization (x-axis). **(F)** Fold change (H3.3 G34R/WT) in the expression of genes associated with at least three lowered enhancers as defined in B is plotted against their percentile. Genes implicated in cell fate determination are highlighted in yellow. p-values of enrichment of up- and down- regulated genes were determined using randomization test. **(G and H)** Immunblots displaying the levels of extopically expressed FLAG-HA tagged various histone transgenes in cells. **(I)** Schematic depicting the hypothesized mechanism by which initial increase of H3K27me3 on H3.3G34W histones may further stimulate PRC2 activity. H3.3G34W histone indirectly (dashed arrow) facilitate PRC2 activity by blocking SETD2. Initial H3K27me3 on the mutated histone further stimulates PRC2 to increase H3K27me2/3 on neighboring nucleosomes (solid arrow). However, K27R substitution in *cis* with G34W mutation disrupts G34W-mediated H3K27me3 and PRC2 stimulation while simultaneously blocking SETD2 activity (lower pannel).

Supplementary Figure 7

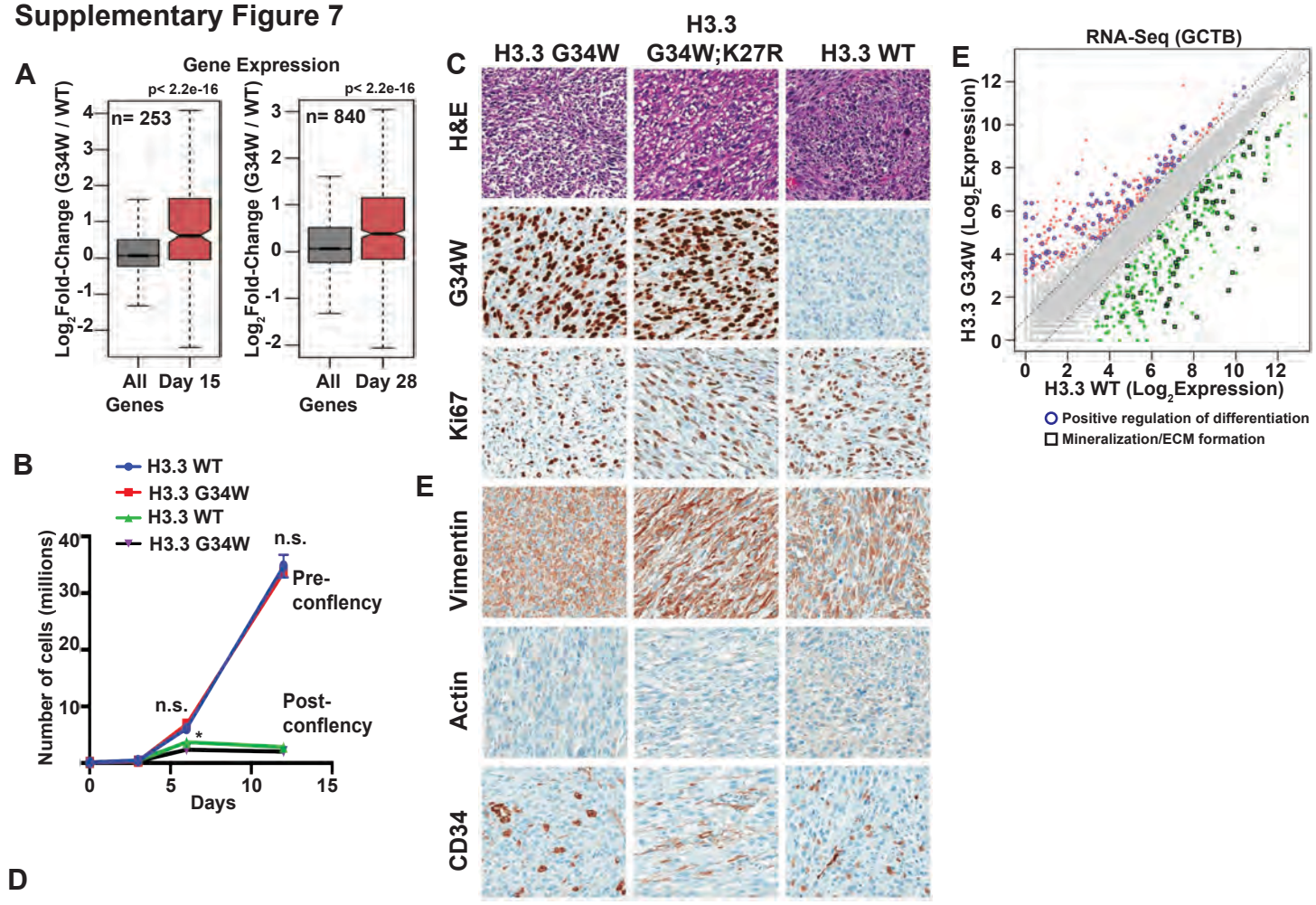

D

	WT	WT	G34W	G34W	G34W-K27R	G34W-K27R
mouse ID	1	3	1	3	1	3
G34W	-	-	+	+	+	+
Vimentin	+	+	+	+	+	+
Actin	Weak + (focal)	Weak +	Weak +	Weak + (patchy)	Weak +	Weak + (patchy)
Desmin	-	-	-	-	-	-
CD34	+	+ (Golgi zone cells)	+ (diffuse, spindle cells)	+ (Golgi zone cells)	+ (spindle cells)	+ (both Golgi and spindle cells)
S100	-	-	-	- (cytoplasmic staining only)	-	-
Sox10	-	-	-	-	-	-
Ki67	98%	85%	98%	70%	98%	95%
H&E	High-grade undifferentiated sarcoma					

Supplementary Figure 7: **(A)** Fold change in the expression of genes that are upregulated upon induction of *in vitro* osteoblasatic differentiation of NIH3T3 cells at day 15 (left, FC > 2) and day 28 (FC >3) (right) in cells expressing H3.3 G34W relative to WT. All genes were used as background. **(B)** *In vitro* proliferation of C3H10T1/2 cells expressing H3.3 WT and H3.3 G34W was monitored for 12 days and is plotted as a function of time. **(C)** Representative images from immunohistochemical characterization of tumor tissues from xenograft mice. **(D)** Summary of pathological features and immunohistochemical studies of tumors from xenograft mice. **(E)** Scatterplot displaying the correlation between gene expression in GCTB-derived stromal cells containing H3.3 WT or G34W mutations. Significantly up-regulated and down-regulated genes are shown in red and green respectively. Genes associated with GO term “positive regulation of differentiation” are marked with blue circles, whereas genes that promote cell-matrix attachment or ECM formation are highlighted with black boxes.

Antibodies

Epitope	Antibody	Application
H3K27me3	CST Cat# 9733, RRID: AB_2616029	ChIP, Immunoblotting
H3K36me3	Active Motif, Cat# 61101, RRID: AB_2615073	ChIP
H3K36me3	CST Cat# 9763, RRID: AB_2616027	ChIP
H3K36me2	CST Cat# 2901, RRID: AB_1030983	ChIP
Brd4	Bethyl Laboratories, Cat# a301-985a50, RRID: AB_2620184	ChIP
Med1	Bethyl Laboratories, Cat# A301-793A, RRID: AB_1211224	ChIP
Rpb1	Sigma, Cat# 8WG16, RRID: AB_11213782	ChIP
FLAG	Cat#F3165, RRID: AB_259529	ChIP
HA	MSKCC, purified in lab	Immunoblotting
H3.3G34W	Developed in collaboration with Sigma Milipore	Immunoblotting

Primers used for qRT-PCR

Gene Name	Forward	Reverse
Hoxb8	TCCAGACCTGGTGCAGTACG	CGGCGGCTGCTTGAGG
Hoxb9	GGATCAAACCAACCCCTCTGC	GCTCCAGCGTCTGGTATTTGG
Cdk6_mRNA	CCTGCTGTGGAAGAAAAGTGC	CTGCGAAACTCCGCCTAGC
igf2bp2_mRNA	CCAGGGCTAAACCTCAGTGC	TCCGGAGTGGGTAGCAAAGG
Sox6	CAAGCCAGGTGATAACTACCCC	GCCACCACCATGTTCAGAGG
Tnfsf15	GCTTCGGGCCATAACAGAAGAG	TCCCAGTGTAGAGCAGAGAGC
Serpina3	GAGTGGAGGAAAAGACAGCAGC	CCAAAGACAGCAGGGGAGAC
A4galt	GCAGGGGGATCTCGTTGG	GCATCCTGGACATGCACACTG
Chd7	GACCCAGGGATGATGAGTCTT	ATGGGGTTCACGGGGTTTTC

ChIP-Seq Normalization Factors

ChIP	H3.3 WT	H3.3 G34W	H3.3 G34R
H3K27me3 reChIP	0.91	1.1	
H3K36me3 reChIP	3.98	4.59	
H3K27ac	0.34	0.44	
H3K27ac for G34R	0.03		0.15
$SETD2^{-/-}$ cells: H3K27ac	4.99	6.15	
$SETD2^{+/+}$ cells: H3K27ac	5.41	7.38	
Brd4	0.06	0.05	
Med1	0.02	0.02	
Ezh2	0.03	3.25	

Supplementary Methods

Animals: Immunodeficient NRG mice (NOD.Cg-Rag1t^{m1Mom} Il2rg^{tm1Wjl}/SzJ) and NSG mice (NOD.Cg-Prkdc^{scid} Il2rg^{tm1Wjl}/SzJ) were purchased from The Jackson Laboratory and used at 8-12 weeks old. One mouse found dead for unknown reasons was excluded from the analysis. No randomization or blinding was used in these experiments. All animal housing and experimental procedures were approved and carried out per the animal resource division of the research institute of the McGill university health center (RI-MUHC) guidelines.

Liquid chromatography-mass spectrometry analysis of histones

Histones (5-10 µg) were resuspended in 100 mM ammonium bicarbonate (pH 8.0), derivatized using propionic anhydride and digested with trypsin as previously described (1). After a second round of propionylation the resulting histone peptides were desalted using C18 Stage Tips, dried using a centrifugal evaporator, and reconstituted in 0.1% formic acid in preparation for LC-MS analysis. Nanoflow liquid chromatography was performed using a Thermo Scientific™ Easy nLC™ 1000 equipped with a 75 µm x 20 cm column packed in-house using Reprosil-Pur C18-AQ (3 µm; Dr. Maisch GmbH, Germany). Buffer A was 0.1% formic acid and Buffer B was 0.1% formic acid in 80% acetonitrile. Peptides were resolved using a two-step linear gradient from 5% to 33% B over 45 min, then from 33% B to 90% B over 10 min at a flow rate of 300 nL/min. The HPLC was coupled online to an Orbitrap Elite mass spectrometer operating in the positive mode using a Nanospray Flex™ Ion Source (Thermo Scientific) at 2.3 kV.

Data-independent acquisition (DIA)

Two full MS scans (m/z 300-1100) were acquired in the orbitrap mass analyzer with a resolution of 120,000 (at 200 m/z) every 8 DIA MS2 scans using isolation windows of 50 m/z each (e.g. 300-350, 350-400…650-700). MS/MS spectra were acquired in the ion trap operating in normal mode. Fragmentation was performed using collision-induced dissociation (CID) in the ion trap mass analyzer with a normalized collision energy of 35. AGC target and maximum injection time were 5e5 and 50 ms for the full MS scan, and 3e4 and 50 ms for the MS/MS can, respectively. Raw files were analyzed using EpiProfile 2.0(2). The area for each modification state of a peptide was normalized against the total peptide signal to give the relative abundance of the histone modification.

Purification of recombinant enzymes

Recombinant PRC2 complex was purified from SF9 cells co-infected with baculoviruses containing human FLAG-tagged EZH2, SUZ12, EED, AEBP2 and RpAp48. Cells were lysed in lysis buffer (15 mM Tris pH8.0, 5 mM MgCl2, 500 mM KCl, 0.5% Triton X-100, 1 mM EDTA, 4 mM PMSF, 1X Protease Inhibitor Cocktail, β-mercaptoethanol), and PRC2 was purified using M2 affinity purification (Sigma Aldrich F1804), followed by anion-exchange chromatography. JARID2 119-574 was expressed in E. coli Rosetta cells. Cells were resuspended in lysis buffer (20 mM HEPES pH 7.9, 500 mM KCl, 1 mM EDTA, 0.8 mM PMSF, 10 mM DTT, 0.01% NP-40) and lysed using tip sonication (30% power, 20 sec ON, 40 sec OFF, 4 cycles). JARID2 was purified from clarified supernatant using Ni-NTA chromatography, followed by cation-exchange chromatography.

GST-fusion proteins with SET domains of SETD2 and NSD2 enzymes were purified from *E. coli* BL21 strain. Cells were induced to express recombinant protein by adding IPTG for 6 hours at 16º C. Cells were resuspended in lysis/wash buffer containing 20 mM HEPES at pH 7.9, 500 mM KCl, 1 mM EDTA, 1 mM DTT, 0.5 mM PMSF, 1X protease inhibitor cocktail and sonicated at 30% amplitude for total 60 sec. After preclearing using centrifugation, lysate was incubated with glutathione beads for 1 hour, washed with lysis/wash buffer and eluted using glutathione.

Reconstitution of recombinant nucleosomes

Recombinant histones were purified from *E. coli* Rosetta cells. Briefly, inclusion bodies were solubilized using 6.3 M Guanidine-HCl, 500 mM NaCl, 50 mM Tris pH 8 and 10 mM β-mercaptoethanol. Histones were purified using Ni-NTA chromatography. Guanidine-HCl was removed using PD10 desalting column and histones were lyophilized overnight. Lyophilized histones were resuspended in D0 buffer (50 mM Tris pH 8.5, 6.3 M Guanidine-HCl, 4 mM EDTA, 10 mM β-mercaptoethanol) and dialyzed against Refolding buffer (20 mM Tris pH 7.5, 1 mM EDTA, 2 M NaCl, 5 mM DTT) for 48 hours with two changes of buffer. Octamers were purified using Superdex 200 column. To reconstitute nucleosomes, octamers and DNA were mixed at 1:1 ratio and dialyzed against 20 mM Tris pH 7.5, 1.4 M NaCl, 1 mM EDTA, 10 mM β-mercaptoethanol for 2 hours. Salt was gradually reduced to 100 mM overnight by pumping Ending buffer at 1ml/min (20 mM Tris pH 7.5, 10 mM NaCl, 1 mM EDTA, 10 mM β-mercaptoethanol). Nucleosomes were finally dialyzed against Ending buffer and stored at -80^{o}C in 10% glycerol.

Chromatin Immunoprecipitation

Cells were cross-linked using 0.8% paraformaldehyde for 5min at room-temperature and quenched with 200 mM glycine. ~20 million cells were lysed by resuspending in digestion buffer

(20 mM Tris pH 7.6, 1mM CaCl2, 0.25% TritonX-100, 5mM PMSF, 1x Protease inhibitor cocktail). Chromatin was treated with 10 units MNase/million cells for 10 min at 37^{o}C to obtain mono-nucleosomes and quenched by adding 5mM EDTA. Chromatin was solubilized by sonication using Covaris (120 Peak incidental power, 5% duty factor, 200 cycles/burst) for 3 minutes. Chromatin was dialyzed against RIPA buffer (10mM Tris pH8, 0.1% SDS, 0.1% Na-DOC, 1 mM EDTA, 1% TritonX-100) for 2 hours. Spike-in (293T or S2 for MSCs) chromatin was added at 1:40 dilution and incubated with antibodies overnight. Chromatin bound to antibody was captured by Dynabeads for 3 hours, washed (3x RIPA, 3x RIPA + 300 mM NaCl, 2x RIPA-LiCl for 8 min each) and eluted in 10 mM Tris, 1 mM EDTA, 1% SDS. Eluted DNA was reverse crosslinked overnight at 65^{o}C, treated with proteinase-K and purified using PCR purification kit.

For Sequential ChIP (reChIP) as optimized previously (3), chromatin from 20 x 10^6 MSCs was incubated with 5 µg of anti-FLAG antibodies (M2 Sigma Aldrich F1804) overnight. For quantitative H3.3-K36me3 reChIP (Figure 2, S5A), chromatin from 293T cells expressing H3.3-HA-FLAG was added at 1:40 dilution prior to addition of anti-FLAG antibody. Antibody bound to chromatin was captured using dynabeads. Washes were performed as described and chromatin bound to beads was eluted using 200 µl of 10mM Tris, 1 mM EDTA, 50 mM NaCl and 0.5 mg/ml 3x-FLAG peptide and diluted with 1 ml of RIPA buffer. reChIP was performed as described in the previous paragraph. Illumina sequencing libraries were generated using NEB Ultra kit.

(Antibodies used for ChIP- H3K27ac: active motif 39133, H3K27me3: cell signaling C36B11, H3K27me2: cell signaling d18C8, H3K36me3: 61101, FLAG: M2 Sigma Aldrich F1804, H3K36me2: Cell signaling 2901S, Brd4: Bethyl Laboratories a301-985a50, RNA Polymerase II: anti-Rpb1 8WG16, Med1: Bethyl Laboratories A301-985A50). Antibodies used for ChIP and primers used for qPCR validation are listed in supplementary table 1. ChIPs for H3K27ac, H3.3K27me3 and H3.3K36me3 were repeated twice with similar results and sequenced. ChIPs for BRD4 and Med1 were performed once but are validated by high correlation between these two different enhancers associated factors and H3K27ac ChIPs.

RNA Isolation and RNA-Seq analysis

Cells were lysed using 800 µl of TriZol reagent and nuclei acid was purified by addition of 160 µl of chloroform and centrifugation. RNA was further purified using RNA isolation kit (IBI Scientific, IB47303) and genomic DNA was removed using DNaseI treatment for 15 min. cDNA was prepared using SuperScript IV VILO mastermix (thermofisher, 11756050) and qRT-PCR was performed using SYBR Green master mix (Applied Biosystems, A25778). Primers used for qRT-PCR are provided in supplementary table 1.

Sequencing libraries were prepared using NEBNext Poly(A) mRNA enrichment kit (New England BioLabs E7490L). RNA from two independent biological replicates were sequenced. Reads that passed quality filter were aligned and expression values were determined using RSEM (4). EBSeq (5) was used to identify differentially expressed genes. Fold-change cutoff of 3-fold was used to define downregulated genes in Figure 4. All genes with PPDE ≥ 0.95 and fold-change ≥ 3 were used to generate heatmap in figure 5A. Heatmap and statistical analyses were performed using R. Gene lists were visualized and annotated using STRING (6). Genes upregulated during *in vitro* osteoblastic differentiation of NIH3t3 cells were used to identify osteoblastic gene expression signature in cells expressing H3.3 G34W (7).

For exogenous normalization, human RNA was added to mouse RNA at 1:50 ratio before mRNA enrichment and library preparation. Sequencing reads were aligned to combined human-mouse transcriptome. After alignment, mouse and human gene expression values were separated. Exogenous normalization factor was determined by median normalization for human genes and was subsequently applied to mouse gene expression values to identify global shift.

Immunohistochemistry (IHC) Xenograft tumors were removed and fixed in 10 % buffered formalin, embedded in paraffin wax and sectioned at a thickness of 5-µm. An automated IHC was performed with Ventana Discovery Ultra. Slides were deparaffinized and rehydrated. Antigen retrieval was done using EDTA buffer. Slides were incubated with the primary Ab. After washing, the secondary Ab was added (anti-Mouse or Rabbit/Mse HRP). After washing, we used DAB kit chromogen to detect the signal.

Supplementary Material and Methods

Sequences for primers used for ChIP-qPCR and RT-qPCR are listed in supplementary reagents and materials.

Normalization factors used for sample normalization in ChIP-Seq experiments are listed in supplementary reagents and materials file.

Supplementary References

1. Sidoli S, Bhanu NV, Karch KR, Wang X, Garcia BA (2016) Complete Workflow for Analysis of Histone Post-translational Modifications Using Bottom-up Mass Spectrometry: From Histone Extraction to Data Analysis. *JoVE* (111):e54112.

2. Yuan Z-F, et al. (2018) EpiProfile 2.0: A Computational Platform for Processing Epi-Proteomics Mass Spectrometry Data. *J Proteome Res* 17(7):2533–2541.
3. Jain SU, et al. (2020) H3 K27M and EZHIP impede H3K27-methylation spreading by inhibiting allosterically stimulated PRC2. *bioRxiv* 35:140–23.
4. Li B, Dewey CN (2011) RSEM: accurate transcript quantification from RNA-Seq data with or without a reference genome. *BMC Bioinformatics* 12(1):323.
5. Leng N, et al. (2013) EBSeq: an empirical Bayes hierarchical model for inference in RNA-seq experiments. *Bioinformatics* 29(8):1035–1043.
6. Szklarczyk D, et al. (2019) STRING v11: protein-protein association networks with increased coverage, supporting functional discovery in genome-wide experimental datasets. *Nucleic Acids Research* 47(D1):D607–D613.
7. Tarkkonen K, Hieta R, Kytölä V, Nykter M, Kiviranta R (2017) Comparative analysis of osteoblast gene expression profiles and Runx2 genomic occupancy of mouse and human osteoblasts in vitro. *Gene* 626:119–131.